Design and Control of a Two-Wheeled Robotic Walker for Balance Enhancement

Airton R. da Silva Jr. and Frank Sup, *Member*, *IEEE*
Department of Mechanical & Industrial Engineering
University of Massachusetts Amherst
Amherst, United States
ardasilv@engin.umass.edu, sup@ecs.umass.edu

***Abstract*—This paper presents the preliminary design results and control strategy of a two-wheeled inverted pendulum (TWIP) robotic walker for assisting mobility-impaired users with balance and stability. A conceptual model of the vehicle is developed and used to illustrate the purpose of this study. Motor dynamics is considered and the linearized equations of motion for the system are derived using Newtonian mechanics. In order to eliminate the effects of loop interaction and impose the desired dynamics on the system, a decoupling control scheme was implemented. Upright stabilization of the robotic walker is achieved using linear quadratic regulator (LQR) control. Improved disturbance rejection is achieved through the implementation of a pitch controller. Simulation results demonstrate that a robustly tuned pitch controller can mitigate effect of disturbance on the linear displacement of the vehicle by as much as 74%.**

Keywords—Wheeled inverted pendulum system, Newtonian mechanics, dynamic modeling, motor dynamics, LQR control, pitch control.

I. INTRODUCTION

RETIREMENT has reached a critical point in the United States with approximately 10,000 baby boomers reaching retirement age every day. In time, many of these elders will start to experience age-associated functional and cognitive impairments that may lead to dependence on mobility aids and personal care assistants in order accomplish basic and instrumental activities of daily living (ADLs). However, with the rising cost of health care and shortages of trained professionals, many industries are turning to intelligent robots in pursuit of an effective solution to some of these challenges.

The overall goal of this research is aimed at the prototype construction and control algorithm development of an intelligent robotic vehicle capable of assisting the elderly as well as mobility-impaired users with balance and stability. To accomplish this goal, the proposed intermediate conceptual model, as shown in Fig. 1, combines the superior maneuverability of a two-wheeled mobile platform with the structural robustness of a four-wheeled system. Accordingly, two modes of operation are possible: two-wheeled and four-wheeled. The ability of the vehicle to transition between these two modes is accomplished by the addition of two symmetrically operated arms. With the integration of two arms, the robotic walker can be used to accommodate a wider range of users with variable assistance needs and help users transfer between sitting and standing positions. A few additional functionalities that become accessible for a two-wheeled inverted pendulum (TWIP) system with two arms include wheelchair mode, advanced fall prevention capabilities, and a four-point base support for added stability while walking.

The actively powered arms are an essential component to making the TWIP robotic walker succeed as a superior substitute for a standard passive walker. However, the primary focus and contribution of this paper is the preliminary development of a control strategy for dictating the behavior of a beneficial self-balancing robotic walker that is suitable for the elderly and mobility-impaired users.

The vehicle drives in reaction to user input forces observed by force sensors placed at the handlebar and utilizes an active impedance scheme to regulate gait and speed based on a set of safety parameters. The active impedance control scheme is shared in both modes of operation but the two-wheeled mode consists of three additional controllers: two LQR controllers and a pitch controller. One of the LQR controllers is dedicated to upright stabilization of the vehicle while the other controls yaw rotation. Meanwhile, the pitch controller adjusts the pitch angle of the robotic walker towards the user based on measured

Fig. 1. Intermediate conceptual model of the TWIP robotic walker.

978-1-4673-6024-1/13/$31.00 ©2013 IEEE

force applied at the handlebars. This leaning action creates a supporting moment against the user which can serve to increase the stability of the device and mitigate external disturbance forces.

Considering the large scale of this research, this paper will only be focusing on the mathematical representation of system dynamics in two-wheeled mode and the development of two controllers: LQR and pitch control. The following section will cover some of the works related to this research.

II. Related Work

A. Personal Mobility Aids and Smart Walkers

Personal mobility aids come in all forms from simple walking canes to fully motorized scooters. For immobile users, the solution is usually a wheelchair. However, if the user has residual mobility capacities, then the solution may be found within mobility devices that provide either wearable augmentation—orthoses and prostheses—or external assistance from canes, crutches, or walkers.

Among the external augmentative mobility devices, there have been various studies conducted on smart walkers that can promote cognitive and physical functioning through sensorial assistance [1-3], active physical support [4, 5], and fall prevention [6]. However, most of these studies were performed on either a three-wheeled or four-wheeled walker with very little research on two-wheeled walking support systems. Recently, Murata Manufacturing has demonstrated a research prototype called the KeePace™. The self-balancing inverted pendulum is intended to be used as a walker. The main challenges in designing a two-wheeled walker that can surpass conventional ones are device safety and load capacity. Our research proposes a potential solution to these challenges and dedicates itself to devising and developing such mobility aid; but first, a proper mathematical description and control scheme for the two-wheeled system is required.

B. Two-Wheeled Inverted Pendulum

Over the past few decades, research on the TWIP system has gained extensive momentum and become increasingly popular with researchers around the world. As a result, a substantial amount of literature on the TWIP is readily available along with a variety of modeling approaches and control methodologies. Some of the approaches that researches have taken to derive the mathematical description of the TWIP model include Newtonian mechanics [7-12], Lagrangian formulation [13-16], and Kane's method [17-19].

The solution to stabilizing an inherently unstable system such as the TWIP can be very complex and diverse. As there is no single control scheme that will perform efficiently for every scenario, there have been distributed efforts in controlling the TWIP system using zero-moment point (ZMP) [7], pole placement [8, 19], LQR [11-14, 17], proportional-integral-derivative (PID) [9, 15, 20], and fuzzy LQR [16]. Although the aforementioned control methodologies were all applied to linearized systems, there has also been a wide range of research dedicated to controlling nonlinear TWIP systems. In Lin *et al.*'s work, the authors developed an effective adaptation of the widely adopted nonlinear control methodology, sliding mode control (SMC) [10]. Another control scheme that can efficiently manage nonlinear systems and perform extremely well under disturbance forces is H∞ robust control [21].

In this paper, two decoupled state-space controllers are developed and evaluated using LQR control. The mathematical description of the system coupled with motor dynamics is derived in Section III. Section IV will address the development of LQR and pitch control. In Section V, simulation results for the LQR and pitch controllers will be analyzed and discussed. Lastly, Section VI will conclude this paper and discuss future work.

III. System Modeling

Prior to developing a controller for the system, a mathematical description must be created to facilitate the process. In this section, vehicle dynamics and motor dynamics will be described in detail. Refer to Table I for a list of the model parameters that will be utilized through the remainder of this section.

Since the research is not yet at the stage of utilizing the two robotic arms, arm dynamics will be ignored in this paper. The physical representation of system dynamics has been simplified to a TWIP with a handlebar and disturbance forces acting at an angle (θ_{LH}, θ_{RH}) on the handlebars (F_{dL}, F_{dR}) and horizontally at the wheels (f_{dL}, f_{dR}) as shown in Fig. 2. Linear displacement of the vehicle is denoted as x, angular rotation about the y-axis (pitch) as θ_P, and angular rotation about the z-axis (yaw) as ψ. The vehicle is actuated by two DC motors which supply torques T_{LW} and T_{RW} to the left and right wheels, respectively.

Using Newtonian mechanics, the equations of motion for the left wheel, which are completely analogous to the right wheel, that will be used to derive the state space representation

TABLE I. Robotic Walker Parameters and Description

Variable	Description	Value	Unit
m_P	Combined mass of the pendulum and chassis	6	kg
m_W	Mass of the wheel	2.3	kg
D_1	Distance between left and right wheels along the y-axis	0.3464	m
D_2	Distance between left and right grip bars along the y-axis	0.35	m
l_{g1}	Distance from point O to the center of mass, *CoM,* of the pendulum	0.40	m
l_1	Length of the pendulum	0.85	m
l_2	Distance from pendulum to grip bar contact point	0.15	m
r	Radius of the wheel	0.1143	m
g	Gravitational acceleration	9.81	m/s^2
J_{P_y}	Combined moment of inertia of the pend. and chassis about the y-axis	0.4339	$kg \cdot m^2$
J_{P_z}	Combined moment of inertia of the pend. and chassis about the z-axis	0.1832	$kg \cdot m^2$
J_W	Moment of inertia of the wheel about the y-axis	0.0144	$kg \cdot m^2$
K_t	Motor's torque constant	0.457	$N \cdot m / A$
K_b	Motor's back EMF constant	0.457	$V / rad / s$
R_a	Motor's armature resistance	3.473	Ω

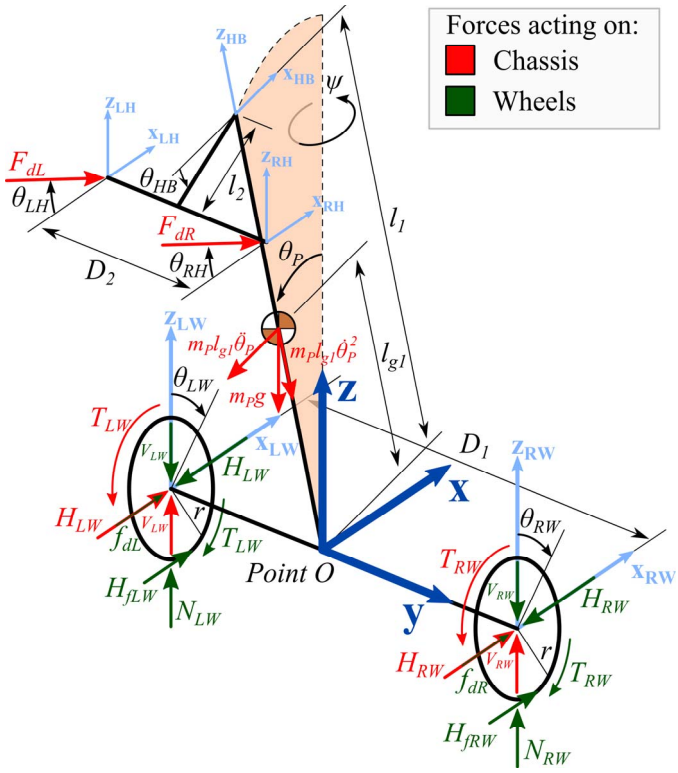

Fig. 2. Diagram of forces and moments acting on the chassis and wheels of the robotic walker.

of the system are as follows:

$$m_W \ddot{x}_{LW} = f_{dL} - H_{LW} + H_{fLW} \tag{1}$$

$$J_W \ddot{\theta}_{LW} = T_{LW} - H_{fLW} r \tag{2}$$

As for the chassis, which includes the pendulum and base of the vehicle, the equations used are:

$$m_P \ddot{x} = H_W - m_P l_{g1} \ddot{\theta}_P \cos\theta_P + m_P l_{g1} \dot{\theta}_P^2 \sin\theta_P + F_d \tag{3}$$

$$\begin{aligned} m_P \ddot{x} \cos\theta_P = {} & H_W \cos\theta_P + V_W \sin\theta_P - m_P g \sin\theta_P \\ & - m_P l_{g1} \ddot{\theta}_P + F_{d_x} \cos\theta_P - F_{d_y} \sin\theta_P \end{aligned} \tag{4}$$

$$\begin{aligned} J_{P_y} \ddot{\theta}_P = {} & -H_W l_{g1} \cos\theta_P - V_W l_{g1} \sin\theta_P - (T_{LW} + T_{RW}) \\ & + F_{d_x} (\eta_1 - l_{g1}) \cos\theta_P - F_{d_x} \eta_2 \sin\theta_P \\ & - F_{d_y} \eta_2 \cos\theta_P - F_{d_y} (\eta_1 - l_{g1}) \sin\theta_P \end{aligned} \tag{5}$$

$$\begin{aligned} J_{P_z} \ddot{\psi} = {} & \frac{D_1}{2} (H_{LW} - H_{RW}) \\ & + \frac{D_2}{2} (F_{dL} \cos\theta_{LH} - F_{dR} \cos\theta_{RH}) \end{aligned} \tag{6}$$

where

$$H_W = H_{LW} + H_{RW} \tag{7}$$

$$V_W = V_{LW} + V_{RW} \tag{8}$$

$$F_{d_x} = F_{dL} \cos\theta_{LH} + F_{dR} \cos\theta_{RH} \tag{9}$$

$$F_{d_y} = F_{dL} \sin\theta_{LH} + F_{dR} \sin\theta_{RH} \tag{10}$$

$$\eta_1 = l_1 - l_2 \sin\theta_{HB} \tag{11}$$

$$\eta_2 = l_2 \cos\theta_{HB} \tag{12}$$

and H_{LW}, H_{RW}, H_{fLW}, H_{fRW}, V_{LW}, and V_{RW} correspond to the reaction forces acting between the chassis, wheels, and ground. To clarify the indices in each subscript, the letters L, R, W, P, g, f, and d stands for left, right, wheel, pendulum, gravity, friction, and disturbance, respectively.

Motor dynamics is derived by first making two assumptions for simplification. Assuming the properties of an ideal DC motor, viscous friction can be neglected. Armature inductance can also be neglected since the electrical time constant ($L_a / R_a \approx 1$ ms) is much smaller than the mechanical dynamics. By applying these assumptions and combining the governing equations of motion for a DC motor, the torque applied at each wheel (T_{LW}, T_{RW}) can be expressed by the following equation:

$$\tau_m = \frac{K_t}{R_a} V_a - \frac{K_t K_b}{R_a} \dot{\theta}_m \tag{13}$$

where τ_m is the motor torque, K_t is the torque constant, R_a is the armature resistance, V_a is the applied voltage to the armature, K_b is the back EMF constant, and $\dot{\theta}_m$ is the rotor's angular velocity. Assuming rigid shaft coupling between the motor and wheels, $\dot{\theta}_m$ can be replaced by wheel angular velocities $\dot{\theta}_{LW}$ and $\dot{\theta}_{RW}$.

For this paper, several additional assumptions that do not significantly compromise the accuracy of simulated results were made. First, it is assumed that wheels are always in contact with the ground and do not slip. Additionally, a linearized version of the nonlinear system can be utilized as long as the simulated pitch angle of the pendulum remains within ±20 degrees of the operating point [22]. Lastly, since the system will be linearized by small angle approximation of θ_P, the moment of inertia of the chassis about the z-axis J_{P_z}, which varies as the pendulum swings back and forth, is assumed to be constant.

By combining equations (1) through (13) and linearizing the resulting nonlinear system of equations at the upright equilibrium point using small angle approximation ($\theta_P = \pi + \phi_P$), the linearized equations are obtained as

$$\begin{aligned} \ddot{x} = {} & \frac{2K_t K_b (m_P l_{g1} r - J_\theta)}{R_a r^2 \alpha} \dot{x} + \frac{m_P^2 g l_{g1}^2}{\alpha} \phi_P + \frac{J_\theta}{\alpha} f_d \\ & + \frac{K_t (J_\theta - m_P l_{g1} r)}{R_a r \alpha} V_a + \frac{(J_\theta \cos\theta_{LH} + m_P l_{g1} \eta_L)}{\alpha} F_{dL} \\ & + \frac{(J_\theta \cos\theta_{RH} + m_P l_{g1} \eta_R)}{\alpha} F_{dR} \end{aligned} \tag{14}$$

$$\ddot{\phi}_P = \frac{2K_tK_b(r\beta - m_Pl_{g1})}{R_ar^2\alpha}\dot{x} + \frac{m_Pgl_{g1}\beta}{\alpha}\phi_P + \frac{m_Pl_{g1}}{\alpha}f_d + \frac{K_t(m_Pl_{g1} - r\beta)}{R_ar\alpha}V_a + \frac{(m_Pl_{g1}\cos\theta_{LH} + \beta\eta_L)}{\alpha}F_{dL} + \frac{(m_Pl_{g1}\cos\theta_{RH} + \beta\eta_R)}{\alpha}F_{dR} \quad (15)$$

$$\ddot{\psi} = \frac{-K_tK_bD_1^2}{2R_ar^2J_\psi}\dot{\psi} + \frac{K_tD_1}{2R_arJ_\psi}(V_{aL} - V_{aR}) + \frac{D_1}{2J_\psi}(f_{dL} - f_{dR}) + \frac{D_2\cos\theta_{LH}}{2J_\psi}F_{dL} - \frac{D_2\cos\theta_{RH}}{2J_\psi}F_{dR} \quad (16)$$

where

$$V_a = V_{aL} + V_{aR} \quad (17)$$

$$f_d = f_{dL} + f_{dR} \quad (18)$$

$$J_\psi = \frac{D_1^2}{2}\left(m_W + \frac{J_W}{r^2}\right) + J_{P_z} \quad (19)$$

$$J_\theta = J_{P_y} + m_Pl_{g1}^2 \quad (20)$$

$$\beta = 2m_W + \frac{2J_W}{r^2} + m_P \quad (21)$$

$$\alpha = J_\theta\beta - m_P^2l_{g1}^2 \quad (22)$$

$$\eta_L = -\eta_1\cos\theta_{LH} + \eta_2\sin\theta_{LH} + (\eta_2\cos\theta_{LH} + \eta_1\sin\theta_{LH})\phi_P \quad (23)$$

$$\eta_R = -\eta_1\cos\theta_{RH} + \eta_2\sin\theta_{RH} + (\eta_2\cos\theta_{RH} + \eta_1\sin\theta_{RH})\phi_P \quad (24)$$

In order to eliminate the effects of loop interaction and impose the desired dynamics on the system, a decoupling controller developed in [8] was implemented. The result is two decoupled state-space equations representing the rotational dynamics of the system about the y-axis (pitch angle) and rotational dynamics of the system about the z-axis (heading angle), respectively,

$$\begin{bmatrix}\dot{x}\\ \ddot{x}\\ \dot{\phi}_P\\ \ddot{\phi}_P\end{bmatrix} = \begin{bmatrix}0 & 1 & 0 & 0\\ 0 & A_{22} & A_{23} & 0\\ 0 & 0 & 0 & 1\\ 0 & A_{42} & A_{43} & 0\end{bmatrix}\begin{bmatrix}x\\ \dot{x}\\ \phi_P\\ \dot{\phi}_P\end{bmatrix} + \begin{bmatrix}0 & 0 & 0 & 0 & 0\\ B_2 & B_{23} & B_{24} & B_{25} & B_{26}\\ 0 & 0 & 0 & 0 & 0\\ B_4 & B_{43} & B_{44} & B_{45} & B_{46}\end{bmatrix}\begin{bmatrix}V_\phi\\ f_{dL}\\ f_{dR}\\ F_{dL}\\ F_{dR}\end{bmatrix} \quad (25)$$

$$\begin{bmatrix}\dot{\psi}\\ \ddot{\psi}\end{bmatrix} = \begin{bmatrix}0 & 1\\ 0 & A_{66}\end{bmatrix}\begin{bmatrix}\psi\\ \dot{\psi}\end{bmatrix} + \begin{bmatrix}0 & 0 & 0 & 0 & 0\\ B_6 & B_{63} & B_{64} & B_{65} & B_{66}\end{bmatrix}\begin{bmatrix}V_\psi\\ f_{dL}\\ f_{dR}\\ F_{dL}\\ F_{dR}\end{bmatrix} \quad (26)$$

where A_{22}, A_{23}, A_{42}, A_{43}, A_{66}, B_2, B_{23}, B_{24}, B_{25}, B_{26}, B_4, B_{43}, B_{44}, B_{45}, B_{46}, B_6, B_{63}, B_{64}, B_{65}, and B_{66} are time invariant functions of the vehicle's parameters.

IV. Control Strategy

The use of a TWIP platform configuration creates delicate control problems that must be carefully addressed. Unlike three-wheeled or four-wheeled walkers, a two-wheeled walker is an inherently unstable system with highly nonlinear dynamics that must be actively balanced to remain upright. In addition to developing a controller to stabilize the system, it is also imperative that the device behaves in a predictable and controllable manner that can promote user stability without inducing risks or creating harm.

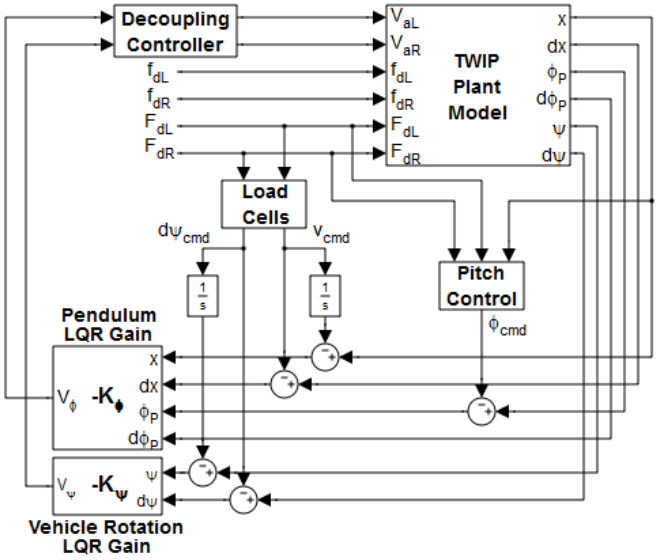

Fig. 3. Control block diagram of robotic walker.

The control scheme developed to balance the robotic walker and implement pitch control is illustrated in Fig. 3. The plant model is represented by the coupled state-space equations which can be obtained from equations (14) through (16). The vehicle will drive along the x-axis at a speed of v_{cmd} when a horizontal force is measured at the handlebar sensors and turn about the z-axis at a rate of $\dot{\psi}_{cmd}$ when there is a difference between measured forces in the left and right grip bars.

The following subsections will be discussing the LQR controller developed along with one of the controllers that are necessary to shape the behavior of a safe and beneficial robotic walker.

A. LQR Controller

The task of the LQR controller is to calculate the optimal state feedback gain matrix **K** that will drive the steady-state error to zero based on a set of constraints defined by the quadratic cost function

$$J = \frac{1}{2}\int_0^\infty \left[\mathbf{x}^T(t)\mathbf{Q}\mathbf{x}(t) + \mathbf{u}^T(t)\mathbf{R}\mathbf{u}(t)\right]dt \quad (27)$$

where **Q** and **R** are symmetric positive-definite matrices that are used to set the relative weights of state deviation and input usage, respectively. Once the relative importance of the control effort (i.e. applied motor voltages V_{aL} and V_{aR}) and steady-state error are specified, the value of this cost function is minimized using the following feedback control law

$$\mathbf{u} = -\mathbf{K}\mathbf{x} \quad (28)$$

Since the disturbance forces acting on the system are uncertainties that cannot be controlled or predicted by the LQR method, all disturbance forces must be omitted from the state-

space equations before calculating the gain matrix. To minimize the cost function and drive the state variables to zero as time goes to infinity, the values for the state **Q** and **R** weighting matrices were tuned by trial and error. While tuning the weighting matrices, the primary objective was to minimize overshoot, settling time, and steady-state error for x and $\dot{x}$. Therefore, the gains for x and $\dot{x}$ were kept relatively high in comparison to the other state variables. For simplicity, only the diagonal entries of the weighting matrices were tuned since the performance of the controller is affected the most when the state and input variables of the system are penalized individually.

B. Pitch Controller

The LQR controller was designed to robustly stabilize the system at its equilibrium point but LQR control by itself is insufficient to achieve the desired behavior from the vehicle. Another step towards achieving the desired system behavior is the implementation of a pitch controller. The purpose of this controller is to mitigate the effect of external disturbance forces acting on the handlebars of the system. Disturbance mitigation is accomplished by adjusting the pitch of the pendulum in order to offset the vehicle's center of mass and generate a counter torque. A secondary purpose for adjusting the pitch of the vehicle is to create a larger distance between the user's feet and the base of the device, allowing the user to take larger steps without hitting the device.

Pitch control is comprised of a simple PID controller that has been designed for disturbance rejection. This controller works by collecting information about the current position of the vehicle along the x-axis and calculating a pitch command ϕ_{cmd} that will drive the difference between current position and desired position to zero. Furthermore, since the pitch controller was strictly designed and tuned to mitigate external disturbance acting on the handlebars, allowing it to operate under different conditions may interfere with the overall performance of the system. Therefore, pitch control has been set to activate only when there is a positive disturbance force acting on the grip bars in the direction aligned with the x-axis.

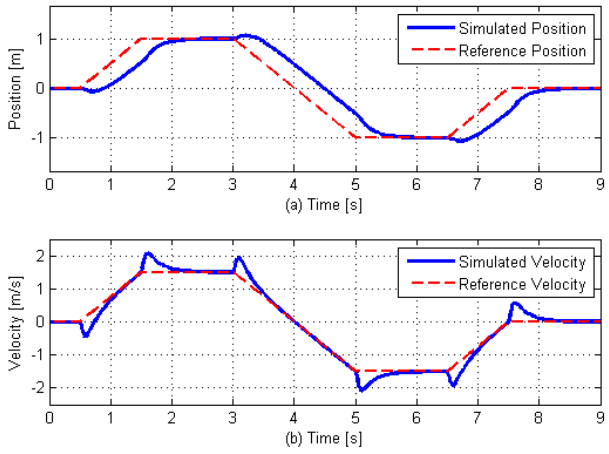

Fig. 4. Simulated performance of LQR controller reacting to (a) position and (b) velocity reference inputs.

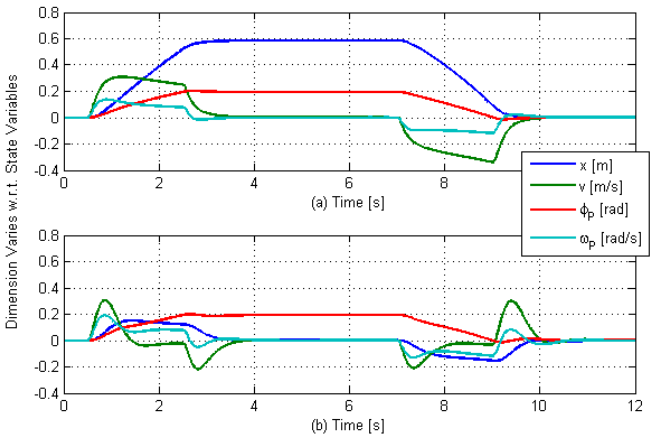

Fig. 5. System response to a 5 N ramp disturbance input acting at the handlebars (a) without and (b) with pitch control.

V. Simulation Results

The model parameters used to simulate the response of the system are listed in Table 1. Additionally, the angle of the handlebar from the axis perpendicular to the pendulum θ_{HB} has been set to 0 degrees while the disturbance force angles (θ_{LH}, θ_{RH}) have been set to 30 degrees.

In order to evaluate the performance of the tuned LQR controller, the response of the system to both a position ramp input and velocity ramp input was investigated as depicted in Fig. 4. The results in Figs. 4a and 4b indicate the LQR controller is very capable of following reference trajectories with minimal overshoot, fast settling time, and nearly zero steady-state error. A minor point of note is the small gap between the specified reference position and simulated position shown in Fig. 4a. This gap is a natural behavior caused by the time required for the vehicle to adjust its pitch before traveling forward or backward. Furthermore, since the LQR controller does not have the ability to read or predict future reference input data, this gap will not be able to converge to the reference position over time. Instead, the gap will remain roughly constant.

The performance of the LQR and pitch controllers while the system is being externally disturbed can be observed in Fig. 5. The external disturbance is a ramp input applied at the handlebars which begins rising at 0.5 seconds into the simulation, saturates at 5 N after 2 s, and begins a 2 s recession back to 0 N at 7 s into the simulation. Fig. 5a shows that using LQR singularly without pitch control causes the vehicle to displace nearly 0.6 m. However, when pitch control is utilized, the maximum displacement of the vehicle is reduced to below 0.2 m, a two-thirds reduction to the maximum vehicle displacement without pitch control. The value of the pitch controller is further reinforced by the fact that it is relatively inexpensive in terms of demanded control effort from the motors as shown in Fig. 6.

However, even with an LQR controller designed for robustness and a pitch controller to augment the ability of the LQR controller to reject external disturbances, the response

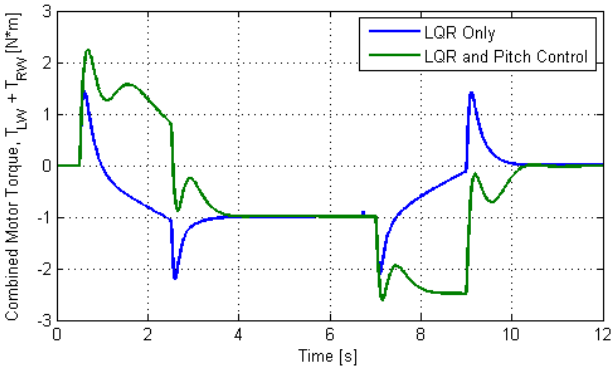

Fig. 6. Motor response to the 5 N ramp disturbance input acting at the handle bars.

observed in the system is still not ideal. In Fig. 5b, there are two 'bumps' along the *x* line, one at the beginning and another at the ending. The vehicle cannot immediately start moving forward or backward from upright position. The time delay necessary to adjust the pitch of the vehicle for moving forward/backward is what causes these 'bumps.' In a robotic walker designed for the mobility-impaired, these 'bumps' could potentially induce user discomfort and debilitating effects on the user's walking stability. However, neither the LQR nor the pitch controller possess the ability estimate or predict future disturbance values. To compensate for this problem, it is recommended to seek a control algorithm that is effective at mitigating immeasurable disturbances.

VI. Conclusion And Future Work

In this paper, we introduced a robotic walker design and developed a robust LQR controller for upright stabilization and disturbance rejection. It was also demonstrated that further disturbance rejection can be accomplished through the implementation of a pitch controller. Simulation results revealed that the pitch controller is capable of reducing the effect of disturbance on the linear displacement of the vehicle by as much as 74%. This estimate is obtained by comparing the peak linear displacements of the vehicle that were simulated in Figs. 5a and 5b.

Although the simulated results are favorable, the combined efforts of the LQR and pitch controllers are still insufficient. Better controller performance is required in order for the vehicle to achieve a behavior that is appropriate for a mobility-impaired user. As a means to improving the overall performance of the system, an effective control scheme for achieving disturbance rejection will be investigated. Along with constructing a prototype to evaluate the performance of the proposed LQR controllers, future work will also focus on controller components that are necessary to create an effective fall prevention system.

References

[1] D. Rodriguez-Losada, F. Matia, A. Jimenez, and R. Galan, "Implementing map based navigation in Guido, the robotic SmartWalker," Proceedings of the 2005 IEEE Inter. Conf. on Robotics and Automation, pp. 3401-3406, 2005.

[2] G. Lee, T. Ohnuma, and N. Y. Chong, "Design and control of JAIST active robotic walker," J. of Intel. Service Robo., 3(3): 125-135, 2010.

[3] C. Barrué, R. Annicchiarico, U. Cortés, A. Martínez-Velasco, E.X. Martín, F. Campana, and C. Caltagirone, "The i-Walker: an intelligent pedestrian mobility aid," European Conf. on Artificial Intelligence, pp. 708-712, 2008.

[4] H.-G. Jun, Y.-Y. Chang, B.-J. Dan, B.-R. Jo, B.-H. Min, H. Yang, W.-K. Song, and J. Kim, "Walking and sit-to-stand support system for elderly and disabled," 2011 IEEE Inter. Conf. on Rehab. Robo., pp. 1-5, 2011.

[5] A. F. Neto, R. Ceres, E. Rocon, and J. L. Pons, "Empowering and assisting natural human mobility: the Simbiosis walker," Inter. J. of Adv. Robotic Sys., Vol. 8, No. 3, pp. 34-50, 2011.

[6] Y. Hirata, S. Komatsuda, and K. Kosuge, "Fall prevention control of passive intelligent walker based on human model," 2008 IEEE/RSJ Int. Conf. on Intelligent Robots and Systems, pp. 1222-1228, 2008.

[7] D. Choi, M. Kim, and J.-H. Oh, "Development of a rapid mobile robot with a multi-degree-of-freedom inverted pendulum using the model-based zero-moment point stabilization method," Advanced Robotics, vol. 26, pp. 515-535, 2012.

[8] F. Grasser, A. D'Arrigo, S. Colombi, and A. C. Rufer, "JOE: A mobile, inverted pendulum," IEEE Trans. on Industrial Electronics, vol. 49, pp. 107-114, 2002.

[9] J. Li, X. Gao, Q. Huang, Q. Du, and X. Duan, "Mechanical design and dynamic modeling of a two-wheeled inverted pendulum mobile robot," 2007 IEEE Inter. Conf. on Auto. and Logistics, pp. 1614-1619, 2007.

[10] S.-C. Lin, C.-C. Tsai, and H.-C. Huang, "Nonlinear adaptive sliding-mode control design for two-wheeled human transportation vehicle," Proc. of the 2009 IEEE Int. Conf. on Systems, Man, and Cybernetics, pp. 1965-1970, 2009.

[11] D. R. Jones and K. A. Stol, "Modelling and stability control of two-wheeled robots in low-traction environments," Australasian Conf. on Robotics and Automation, 2010.

[12] S. Kalra, D. Patel, and K. Stol, "Design and hybrid control of a two wheeled robotic platform," In Proc. 2007 Australasian Conf. on Robotics and Automation, 2007.

[13] S. H. Jeong and T. Takahashi, "Wheeled inverted pendulum type assistant robot: inverted mobile, standing, and sitting motions," Proc. of the 2007 IEEE/RSJ Int. Conf. on Intelligent Robots and Systems, pp. 1932-1937, 2007.

[14] C. Xu, M. Li, and F. Pan, "The system design and LQR control of a two-wheels self-balancing mobile robot," Int. Conf. on Electrical and Control Engineering, pp. 2786-2789, 2011.

[15] K. M. Goher and M. O. Tokhi, "Development, modeling and control of a novel design of two-wheeled machines," Journal of Selected Areas in Robotics and Control, pp. 6-16, 2010.

[16] R. Kahani and B. Moaveni, "Control of two-wheels inverted pendulum using parallel distributed compensation and fuzzy linear quadratic regulator," 2011 3rd Int. Conf. on Computer Modeling and Simulation, vol. 2, pp. 312-317, 2011.

[17] Y. Kim, S. H. Kim, and Y. K. Kwak, "Dynamic analysis of a nonholonomic two-wheeled inverted pendulum robot," Journal of Intelligent and Robotic Systems, vol. 44, pp. 25-46, 2005.

[18] M. Muhammad, S. Buyamin, M. N. Ahmad, and S. W. Nawawi, "Dynamic modeling and analysis of a two-wheeled inverted pendulum robot," 2011 Third Int. Conf. on Computational Intelligence, Modelling & Simulation, pp. 159-164, 2011.

[19] S. W. Nawawi, M. N. Ahmad, and J. H. S. Osman, "Development of a two-wheeled inverted pendulum mobile robot," The 5th Student Conf. on Research and Development, 2007.

[20] S. J. Lee, Y. G. Bae, and S. Jung, "Object handling control between a balancing robot and a human operator," 2012 IEEE Int. Symposium on Industrial Electronics, pp. 931-936, 2012.

[21] X. Ruan and J. Chen, "H∞ robust control of self-balancing two-wheeled robot," Proc. of the 8th World Congress on Intelligent Control and Automation, pp. 6524-6527, 2010.

[22] D. Choi and J.-H. Oh, "Human-friendly motion control of a wheeled inverted pendulum by reduced-order disturbance observer," 2008 IEEE Int. Conf. on Robotics and Automation, pp. 2521-2526, 2008.